

Correlation Analyses on Binding Affinity of Sialic Acid Analogues and Anti-Influenza Drugs with Human Neuraminidase Using *ab Initio* MO Calculations on Their Complex Structures — LERE-QSAR Analysis (IV)

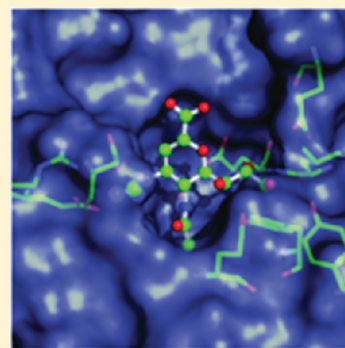
Seiji Hitaoka,[†] Hiroshi Matoba,[†] Masataka Harada,[†] Tatsusada Yoshida,[†] Daisuke Tsuji,[†] Takatsugu Hirokawa,[‡] Kohji Itoh,[†] and Hiroshi Chuman^{*,†}

[†]Institute of Health Biosciences, The University of Tokushima Graduate School, 1-78 Shomachi, Tokushima 770-8505, Japan

[‡]Computational Biology Research Center (CBRC), National Institute of Advanced Industrial Science and Technology (AIST), 2-42 Aomi, Koto-ku, Tokyo 135-0064, Japan

S Supporting Information

ABSTRACT: We carried out full *ab initio* fragment molecular orbital (FMO) calculations for complexes comprising human neuraminidase-2 (hNEU2) and sialic acid analogues including anti-influenza drugs zanamivir (Relenza) and oseltamivir (Tamiflu) in order to examine the variation in the observed inhibitory activity toward hNEU2 at the atomic and electronic levels. We recently proposed the LERE (linear expression by representative energy terms)-QSAR (quantitative structure–activity relationship) procedure. LERE-QSAR analysis quantitatively revealed that the complex formation is driven by hydrogen-bonding and electrostatic interaction of hNEU2 with sialic acid analogues. The most potent inhibitory activity, that of zanamivir, is attributable to the strong electrostatic interaction of a positively charged guanidino group in zanamivir with negatively charged amino acid residues in hNEU2. After we confirmed that the variation in the observed inhibitory activity among sialic acid analogues is excellently reproducible with the LERE-QSAR equation, we examined the reason for the remarkable difference between the inhibitory potencies of oseltamivir as to hNEU2 and influenza A virus neuraminidase-1 (N1-NA). Several amino acid residues in close contact with a positively charged amino group in oseltamivir are different between hNEU2 and N1-NA. FMO-IFIE (interfragment interaction energy) analysis showed that the difference in amino acid residues causes a remarkably large difference between the overall interaction energies of oseltamivir with hNEU2 and N1-NA. The current results will be useful for the development of new anti-influenza drugs with high selectivity and without the risk of adverse side effects.



1. INTRODUCTION

Neuraminidases (NAs, also called sialidases) are ubiquitous exoglycosylhydrolases that hydrolyze the terminal sialic acids of glycoproteins, glycopeptides, gangliosides, oligosaccharides, and polysaccharides and have been proved to play important roles in various biological processes through regulation of cellular sialic acid contents. NAs are widely distributed in nature, from viruses, and microorganisms such as bacteria, protozoa, and fungi to higher animals and humans.¹ Structural and functional studies on NAs have been widely reported so far. Most of them were on influenza virus NAs,^{2–4} a smaller number on human neuraminidases (hNEUs) having also been reported.^{5–8} The NA inhibitor first developed, 2-deoxy-2,3-didehydro-*N*-acetyl-neuraminic acid (Neu5Ac2en, DANA),⁹ was designed as a putative transition state analogue of sialic acid in the late 1960s. Although the inhibition by DANA is not selective for influenza virus NAs,^{10,11} DANA shows moderate inhibitory activity toward a variety of NAs, suggesting that amino acid residues in the active sites of NAs are highly conserved among a number of species including influenza virus and human NAs.

hNEUs are classified into four types,¹² the lysosomal neuraminidase (hNEU1),¹³ cytosolic neuraminidase (hNEU2),¹⁴

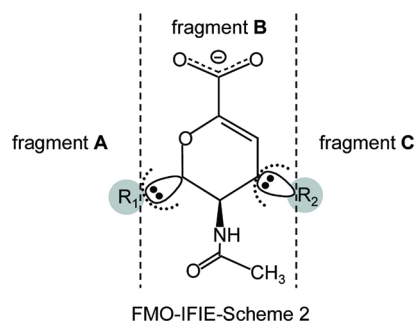
plasma membrane-associated neuraminidase (hNEU3),¹⁵ and lysosomal/mitochondrial membrane-associated neuraminidase (hNEU4),¹⁶ according to several characteristics, such as their subcellular distributions, enzymatic properties, and substrate specificities. They are involved in various cellular functions such as cell proliferation, differentiation, and apoptosis.¹⁷ hNEU1 is essential for the lysosomal catabolism of sialylated glycoconjugates,^{18–20} hNEU2 is able to recognize not only sialosyl linkages but also saccharide units close to sialic acids and the supramolecular organization of such as gangliosides, hNEU3 is expected to be involved in cell surface functions by modulating gangliosides, and hNEU4 is active against a broad range of sialylated glycoconjugates and has been implicated in the catabolism of glycolipids, but the details are not known at present. The crystallographic structure of hNEU2²¹ is the only available one among those of the four hNEUs.

As mentioned previously, DANA inhibits influenza virus NAs moderately but is not used as an anti-influenza drug because of its practically low potency. Through structure-based approaches

Received: May 27, 2011

Published: August 28, 2011

Table 1. Chemical Structure and Inhibitory Potency of Compounds 1–5 against hNEU2



compound no.	name	R ₁ (fragment A)	R ₂ (fragment C)	hNEU2 log K _i ^d
1	IEM ^b	OCH ₂ CH(CH ₃) ₂	OH	−3.06
2	HEM ^c	OCH ₂ CH ₂ CH ₂ (OH ¹)	OH	−3.13
3	DEM ^d	OCH ₂ CH(OH ¹)CH ₂ (OH ²)	OH	−2.85
4	DANA ^e	CH(OH ¹)CH(OH ²)CH ₂ (OH ³)	OH	−3.85
5	zanamivir	CH(OH ¹)CH(OH ²)CH ₂ (OH ³)	NHC(=NH ₂ ⁺)NH ₂	−4.77

^a Taken from ref 33. ^b Isobutyl ether DANA mimetic. ^c 3-Hydroxypropyl ether DANA mimetic. ^d 2,3-Dihydroxypropyl ether DANA mimetic. ^e 2-Deoxy-2,3-didehydro-*N*-acetyl-neuraminic acid.

and the structure–activity relationships (SAR) of analogues of DANA, four anti-influenza drugs have been developed so far: zanamivir (Relenza),²² oseltamivir (Tamiflu),²³ peramivir (Rapiacta),²⁴ and laninamivir (Inavir).²⁵ These drugs have the potential to affect the activities of endogenous hNEUs, which can recognize similar substrates. Indeed, zanamivir and oseltamivir have been reported to inhibit hNEUs at the micromolar level or more, while they exhibit inhibitory activity in the nanomolar range against influenza virus NAs.²⁶ Over a thousand adverse events have been reported so far to have occurred with the use of oseltamivir, including a small number of rare but severe neuropsychiatric adverse events, especially in children.²⁷ Therefore, it is of great importance to elucidate the differences in sensitivity to these anti-influenza drugs among human and influenza virus NAs from the aspect of the inhibitory interaction mechanism at the atomic and electronic levels.

We previously reported correlation analyses of the interaction energies of influenza A virus neuraminidase-1 (N1-NA) with a series of eight sialic acid analogues including oseltamivir involving *ab initio* FMO (fragment molecular orbital)-IFIE (interfragment interaction energy) calculations at the Møller–Plesset (MP2) level.²⁸ Our previous study revealed that the dispersion and/or hydrophobic interaction energies of the alkoxy side chain in each ligand with several amino acid residues in N1-NA, which surrounds the former, govern the overall free-energy change in the binding interaction. Recently, we proposed a novel quantitative structure–activity relationship (QSAR) procedure called linear expression by representative energy terms (LERE) involving molecular calculations such as *ab initio* FMO and generalized Born/surface area (GB/SA) ones.^{29,30} The proposed LERE-QSAR procedure was demonstrated to provide detailed quantitative information as to the ligand–protein interaction of carbonic anhydrase with a series of substituted benzenesulfonamides at the atomic and electronic levels, which cannot be obtained with any other procedures.

There are a small number of compounds of which the inhibitory potency against hNEU2 have been measured and reported.^{26,31–34}

In this work, we constructed complexes of hNEU2 with six sialic acid analogues exhibiting relatively potent inhibitory activity, zanamivir, oseltamivir, DANA, and three analogues of DANA, by using molecular mechanics calculations and then carried out *ab initio* FMO and continuum solvation model calculations for each complex structure. Subsequently, we performed LERE-QSAR analysis and quantitatively examined the binding mechanism at the atomic and electronic levels. Finally, we discuss the observed difference between the sensitivities of oseltamivir to hNEU2 and N1-NA in terms of structure and interaction energy.

2. METHODS

2.1. Compound Set. Table 1 shows the chemical structures of four sialic acid analogues [IEM (compound 1), HEM, (2), DEM (3), and DANA (4)] and an anti-influenza drug, zanamivir (5), along with their inhibitory constants *K_i* against hNEU2.³³ Compounds 1–4 have a hydroxyl group as a common substituent (R₂, fragment C) and variable substituents (R₁, fragment A), hydroxyl groups existing in compounds 2–4. Compounds 4 and 5 have an identical substituent R₁, but compound 5 has a guanidino group (NHC(=NH₂⁺)NH₂) in fragment C, instead of the hydroxyl one of compounds 1–4. Thus, a total of five compounds with the common skeletal structure of 3-acetamido-3,4-dihydro-2*H*-pyran-6-carboxylic acid (fragment B) were subjected to analyses. Another anti-influenza drug, oseltamivir (compound 6), was added to the above compound set in Section 3.2.

2.2. Modeling of Complex Structures. The X-ray structures of complexes of hNEU2 with compounds 1 (PDB code: 2F11, complex 1), 2 (2F12, complex 2), 3 (2F13, complex 3), 4 (DANA, 1VCU, complex 4), and 5 (zanamivir, 2F0Z, complex 5) are all available. The structure of hNEU2 varies slightly among the crystallographic structures of complexes 1–5. The initial geometries of complexes 1–3 and 5 were taken from the crystallographic structure of complex 4 having a minimum number of missing residues, by replacing DANA in complex 4 with each of compounds 1–3 and 5. Loops A (Ile103–Thr122) and B

(Val265–Ser275) in hNEU2 are located in the vicinity of fragment A in compound 4. Loops A and B in the crystallographic structure of complex 5 occupy very close positions to those in complex 4, respectively. However, loops A and B in the crystallographic structure of complex 2 take on significantly different positions from those in complexes 4 and 5. Although several amino acid residues in loop A are not found (missing residues) in the crystallographic structures of complexes 1 and 3, the atomic positions of the corresponding amino acid residues other than the missing ones are nearly the same among the crystallographic structures of complexes 1, 2, and 3. Therefore, the initial geometries of complexes 1–3 were reconstructed by replacing loops A and B in the crystallographic structure of complex 4 with those in the crystallographic one of complex 2.

In our previous work,²⁸ we showed that two crystal water molecules inside the active site of N1-NA play an important role in the binding interaction: ligands having guanidino and amino groups in fragment C bind with only one water molecule (W1) and with two molecules (W1 and W2), respectively. The X-ray structures of nine complexes of hNEU2 with ligands (PDB codes: 2F11, 2F12, 2F13, 2F25 (dimer), 2F27 (dimer), and 1VCU (dimer)) were carefully examined. The root-mean-square deviation values for the atomic positions of W1 and W2 are both within 0.44 Å, indicating that their positions were nearly fixed. W1 and W2 for complexes 1–4 and W1 for complex 5 were placed at the respective average positions determined by the above procedure. Five and four sodium ions (Na⁺) were added to neutralize the total −5 and −4 charge of the complexes of hNEU2 with negatively charged ligands (compounds 1–4) and with neutral ones (compounds 5 and 6), respectively. Each complex was then solvated in a truncated octahedral box of TIP3P waters extending 12 Å from hNEU2.

Three-step energy minimizations were performed as follows: (i) hydrogen atoms, (ii) water molecules and counterions, and (iii) the entire system were sequentially relaxed for 2000, 6000, and 6000 steps, respectively. During these minimizations, the atomic positions of Glu111, Tyr179, Tyr181, Glu218, and Gln270, which could be involved in electrostatic and/or hydrogen-bonding interactions with fragment A in compounds 1–5, were constrained with a harmonic potential of 10 kcal/mol/Å². The finally obtained energy minimized complex structures were used in the following calculations. All molecular mechanics calculations were carried out using the AMBER10 package³⁵ with parameters of parm99³⁶ and general AMBER force field (GAFF)³⁷ for hNEU2 and each compound, respectively. The X-ray structures of compounds 1–5 bound with hNEU2 were subjected to partial geometry optimization (bond lengths and angles), fixing dihedral angles to the corresponding X-ray ones with HF/6-31G* calculations (Gaussian03 program³⁸). Similarly, that of compound 6 bound with N1-NA was geometry optimized. Then, partial atomic charges in each compound were determined according to the restrained electrostatic potential (RESP) fitting procedure^{39–41} with HF/6-31G* calculations. The atomic charges in compounds 1–6 are consistent with those of atoms in amino acid residues, because the latter charges were determined with the same procedure in the Amber (parm99) force field generally used for proteins.^{36,37} Atom names, atom types, and partial atomic charges of compounds 1–6 are listed in Table S1 (Supporting Information). The summation of partial atomic charges q within each fragment [$\sum q_i$ (X) (summation over atoms in fragment X), X = A, B, and C] for zanamivir

(compound 5) and oseltamivir (compound 6) is similar with that reported by Udommaneethanakit et al.⁴¹

2.3. LERE Formalism. We recently proposed LERE analysis involving molecular calculations such as the ab initio FMO and GB/SA ones and reported LERE-QSAR analyses of a series of substituted benzenesulfonamides with bovine carbonic anhydrase.^{29,30}

A basic assumption when dissecting free-energy terms is that they are all additive^{28,42,43}

$$\Delta G_{\text{obs}} = \Delta G_{\text{bind}} + \Delta G_{\text{sol}} + \Delta G_{\text{dis}} + \Delta G_{\text{others}} \quad (\text{I})$$

ΔG_{obs} on the left-hand side of eq I is the overall free-energy change obtained from the observed inhibitory constant K_i : $\Delta G_{\text{obs}} = 2.303 RT \log K_i$ ($T = 310$ K). ΔG_{bind} , ΔG_{sol} , and ΔG_{dis} in eq I are the intrinsic interaction energy between an inhibitor and protein, the solvation free-energy change associated with complex formation, and the dissociation free-energy change of an inhibitor, respectively. ΔG_{others} , which represents the sum of free-energy terms such as the deformation energies of a protein and ligand other than ΔG_{bind} , ΔG_{sol} , and ΔG_{dis} , is assumed to be linear with the sum of representative free-energy terms ΔG_{bind} , ΔG_{sol} , and ΔG_{dis} in eq I, and ΔG_{others} is expected to act as a penalty term ($\beta < 0$), i.e., LERE approximation

$$\Delta G_{\text{others}} = \beta(\Delta G_{\text{bind}} + \Delta G_{\text{sol}} + \Delta G_{\text{dis}}) + \text{const (LERE approximation)} \quad (\text{II})$$

During complex formation between compounds 1–5 and hNEU2, ΔG_{dis} does not need to be considered in the current case, because a carboxylate group common to compounds 1–5 and a guanidino one in compound 5 take on nearly complete ionized forms [COO^- ($\text{p}K_a \sim 2.4$) and $\text{NHC}(=\text{NH}_2^+)\text{NH}_2$ ($\text{p}K_a \sim 13$), respectively] before and after complex formation at experimental pH = 5.6.^{33,44}

ΔG_{obs} very probably exhibits a ubiquitous energetic relation on complex formation between a protein and a series of ligands having a similar structure, the entropy–enthalpy compensation rule^{45–48}

$$T\Delta S_{\text{obs}} = \alpha\Delta H_{\text{obs}} + \text{const (entropy–enthalpy compensation)} \quad (\text{IIa})$$

The value of α ($\alpha > 0$) on complex formation between a sialic acid analogue and hNEU2 is supposed to be within the range of 0.70 ± 0.20 , judging from the results of isothermal titration calorimetry (ITC) experiments on complex formation of various sugars and sugar mimetics with their binding proteins.^{49–52} Frederick et al.⁵³ showed that a change in the protein conformational entropy (ΔS_{bind} , which includes changes in the vibrational, rotational, and translational entropies) is linearly correlated with a change in overall entropy on the formation of complexes of calmodulin with its binding peptides, using nuclear magnetic resonance (NMR) relaxation methods. They proposed the possibility that ΔS_{bind} makes a major contribution to the overall binding entropy change. In the case where the complex formation is mostly driven by the electrostatic interaction energy between a charged ligand and protein, the intrinsic binding enthalpy term ΔH_{bind} and the polar component of solvation free-energy change $\Delta G_{\text{sol}}^{\text{pol}}$, calculated with continuum solvation models such as the generalized Born (GB) and Poisson–Boltzmann (PB) ones, are probably major contributors to the overall free-energy changes. Avbelj et al.⁵⁴ recently showed that the observed solvation (hydration) free-energy changes of the polar parts in several dipeptides consist mostly of the enthalpy term arising

from the electrostatic interaction, the energy of which can be well reproduced with PB type calculation. Directly from the original Born equation: $\Delta G_{\text{sol}}^{\text{pol}} = -(q^2/2r)(1 - 1/\epsilon)$, the enthalpy change is given by the expression: $\Delta H_{\text{sol}} = \Delta G_{\text{sol}}^{\text{pol}} - T(\partial G_{\text{sol}}^{\text{pol}}/\partial T)_P = -(q^2/2r)[1 - 1/\epsilon - (T/\epsilon^2)(\partial\epsilon/\partial T)_P]$, where r , q , ϵ , and T are the cavity radius formed by the ion in a particular solvent, ion charge, dielectric constant, and temperature, respectively.^{55,56} The reported value of $[(T/\epsilon)(\partial\epsilon/\partial T)_P]$ for water ($\epsilon = 78.4$) at 298 K is -1.357 ,⁵⁵ giving 0.983 for the ratio between $\Delta G_{\text{sol}}^{\text{pol}}$ and ΔH_{sol} ($\Delta G_{\text{sol}}^{\text{pol}}/\Delta H_{\text{sol}} = 0.983$). The ratio close to unity suggests that ΔH_{sol} is generally replaceable by $\Delta G_{\text{sol}}^{\text{pol}}$ with satisfactory accuracy. We showed the possibility that the energy term (E_{sol}) calculated with the ab initio MO-continuum solvation model (COSMO) corresponds to the effective enthalpic energy term associated with the partition equilibrium between the aqueous and organic solvent phases rather than the overall solvation free-energy term, when we analyzed more than 200 $\log P_{\text{sol/w}}$ values.⁵⁷

ΔH_{bind} can be replaced by ΔE_{bind} because of the lack of significant volume and pressure changes in solution. ΔE_{bind} consists of $\Delta E_{\text{bind}}^{\text{HF}}$ and E^{disp} , which are the intrinsic binding energy at the Hartree–Fock (HF) level and the dispersion (van der Waals) energy, respectively. ΔG_{sol} consists of $\Delta G_{\text{sol}}^{\text{pol}}$ and the nonpolar free-energy change $\Delta G_{\text{sol}}^{\text{nonpol}}$. $\Delta E_{\text{bind}}^{\text{HF}}$ and $\Delta G_{\text{sol}}^{\text{pol}}$ are considered to be “electrostatic energy terms”⁵⁸ involved in the electrostatic interactions among a ligand, protein, and solvent medium. E^{disp} and $\Delta G_{\text{sol}}^{\text{nonpol}}$ are considered to be “local energy terms”, which are effective only at a short distance. We reported that $\Delta G_{\text{sol}}^{\text{pol}}$ shows an excellent anticorrelation with $\Delta E_{\text{bind}}^{\text{HF}}$ during complex formation between carbonic anhydrase and a series of substituted benzenesulfonamides.^{29,30} We assumed that the sum of the electrostatic energy terms represents the effective overall enthalpic change, i.e., the effective binding enthalpy change in a solvent, $\Delta H_{\text{bind}}^{\text{sol}} = \Delta E_{\text{bind}}^{\text{HF}} + \Delta G_{\text{sol}}^{\text{pol}}$, on the condition that contributions from the local energy terms to $\Delta H_{\text{bind}}^{\text{sol}}$ are significantly smaller than those from the electrostatic ones. This condition is equivalent to that the statistical variances of E^{disp} and $\Delta G_{\text{sol}}^{\text{nonpol}}$ are negligibly smaller than those of $\Delta E_{\text{bind}}^{\text{HF}}$ and $\Delta G_{\text{sol}}^{\text{pol}}$ in a correlation equation. The entropy–enthalpy compensation is now expressed as

$$T\Delta S_{\text{bind}}^{\text{sol}} = \alpha(\Delta E_{\text{bind}}^{\text{HF}} + \Delta G_{\text{sol}}^{\text{pol}}) + \text{const} \quad (\text{III})$$

Assuming eq III, the effective overall free-energy change $\Delta G_{\text{bind}}^{\text{sol}}$ is expressed as $(1 - \alpha)(\Delta E_{\text{bind}}^{\text{HF}} + \Delta G_{\text{sol}}^{\text{pol}}) + \text{const}$. Although the protein conformational entropic term ($T\Delta S_{\text{bind}}$) is often estimated using normal mode and molecular dynamics calculations, the calculated one is known to exhibit significant large uncertainties.^{59–61} Alternatively, eqs I, II, and III yield eq IV without estimation of $T\Delta S_{\text{bind}}$ ^{62,63} directly

$$\Delta G_{\text{obs}} = (1 + \beta)(1 - \alpha)(\Delta E_{\text{bind}}^{\text{HF}} + \Delta G_{\text{sol}}^{\text{pol}}) + \text{const} \quad (\text{IV})$$

Equation IV appears to take a similar form to the solvated interaction energy (SIE) model proposed by Naïm et al.⁶⁴ Although they introduced several adjusting parameters such as the effective interior dielectric constant in order to adjust the calculated overall free-energy change to the observed one, eq IV has only two scaling factors, α and β , which effectively and naturally consider the entropy–enthalpy compensation and penalty effects, respectively. It is obvious but noteworthy that the α and β values depend on a set of a series of ligands and their target proteins. Also, it should be noted that the above procedure is probably applicable

to a congeneric series of ligands having the same skeleton but probably not to a set containing structurally diverse ones.

2.4. Calculation of Representative Energy Terms. $\Delta E_{\text{bind}}^{\text{HF}}$ ($= E^{\text{HF}}(\text{complex}) - [E^{\text{HF}}(\text{protein}) + E^{\text{HF}}(\text{ligand})]$) and E^{disp} ($= \Delta E_{\text{bind}}^{\text{MP2}} - \Delta E_{\text{bind}}^{\text{HF}}$) were calculated using ab initio fragment molecular orbital (FMO) calculations with one residue (including W1 and W2) per FMO-fragment partition (FMO-IFIE-Scheme 1)^{65–68} at the HF and MP2/6-31G levels, respectively, using the ABINIT-MP program.^{69,70} Our previous studies involving FMO calculations^{28–30,71,72} demonstrated that interfragment interaction energy (IFIE) analysis can provide valuable information independent from that obtained with the LERE-QSAR one. In the present work, the structures of compounds 1–5 were further divided into three FMO-fragments A, B, and C (FMO-IFIE-Scheme 2, shown in Table 1),^{28,73–75} in order to clarify the contribution of each fragment to the overall interaction energy. Amino acid residues, which are closely located in fragments A, B, and C, are denoted by pockets A, B, and C, respectively. IFIE^{HF} (fragment X, Y) denotes the IFIE value between X (fragment X in a ligand) and Y (amino acid residue Y in a protein) at the HF level, and $\Sigma\text{IFIE}^{\text{HF}}$ (fragment X, pocket Z) represents summation of IFIE^{HF} (fragment X, Y) over all the amino acid residues Y in pocket Z. As expected,^{28,29,71,72} $\Delta E_{\text{bind}}^{\text{HF}}$ is almost completely linear with $\Sigma\text{IFIE}^{\text{HF}}$ (fragment X, pocket Z) (summation over X, Z = A, B, and C) for compounds 1–5 ($r = 0.999$). This fact guarantees that the total intrinsic binding energy can be decomposed into local fragment–pocket interaction energies. The solvation free-energy terms $\Delta G_{\text{sol}}^{\text{pol}}$ and $\Delta G_{\text{sol}}^{\text{nonpol}}$ were calculated with the molecular dynamics (MD)–PB/SA (Poisson–Boltzmann/surface area) and MD–GB/SA (generalized Born/surface area) procedures^{76,77} included in the AMBER10 package. These terms were obtained as ensemble averages of snapshot structures in the MD trajectory, $\langle G_{\text{sol}}^{\text{pol}}(\text{PB}) \rangle$, $\langle G_{\text{sol}}^{\text{pol}}(\text{GB}) \rangle$, and $\langle G_{\text{sol}}^{\text{nonpol}} \rangle$. It is necessary to average G_{sol} , because $G_{\text{sol}}^{\text{pol}}$ is supposed to be sensitive to subtle conformational changes occurring in domains other than the binding one.^{62,63,78,79} Short-time MD with 200 ps of a production run at 300 K was performed to refine each complex structure (structure annealing), and snapshot structures were collected for the last 150 ps trajectory at 3.0 ps intervals. We confirmed that $\langle \Delta G_{\text{sol}}^{\text{pol}}(\text{PB}) \rangle$ and $\langle \Delta G_{\text{sol}}^{\text{pol}}(\text{GB}) \rangle$ were not significantly changed during a longer simulation time, by performing 1 and 10 ns simulations for (1) the complex of hNEU2 with compound 4 and (2) that of N1-NA with compound 6, respectively. The absolute differences of $\langle \Delta G_{\text{sol}}^{\text{pol}} \rangle$ between the 200 ps and longer time simulations are less than 1.4 and 3.3 kcal/mol for (1) and (2), respectively.

3. RESULTS AND DISCUSSION

3.1. LERE-QSAR Analysis of Complex Formation of hNEU2 with Sialic Acid Analogues and Zanamivir. Table 2 lists the observed and calculated overall free-energy changes along with the electrostatic interaction energy terms $\Delta E_{\text{bind}}^{\text{HF}}$ and $\langle \Delta G_{\text{sol}}^{\text{pol}} \rangle$, and the local interaction energy terms E^{disp} and $\langle \Delta G_{\text{sol}}^{\text{nonpol}} \rangle$, of compounds 1–5 listed in Table 1. Figure 1 shows the variations in these energy terms. The variances of $\Delta E_{\text{bind}}^{\text{HF}}$ and $\langle \Delta G_{\text{sol}}^{\text{pol}}(\text{PB}) \rangle$, which mainly arise from the electrostatic interaction, are considerably large (3989 and 1967 kcal²/mol², respectively). On the other hand, those of E^{disp} and $\langle \Delta G_{\text{sol}}^{\text{nonpol}} \rangle$ are much smaller (5.06 and 0.01 kcal²/mol², respectively). Thus, the variation in overall free-energy change is governed by $\Delta E_{\text{bind}}^{\text{HF}}$ and $\langle \Delta G_{\text{sol}}^{\text{pol}}(\text{PB}) \rangle$, satisfying the condition for eq IV.

Table 2. Overall Free-Energy Change ΔG and Representative Energy Terms^a (hNEU2)

compound									
no.	name	ΔG_{obs}^b	ΔG_{calc}^c	ΔG_{calc}^d	$\Delta E_{\text{bind}}^{\text{HF}}$	$\langle \Delta G_{\text{sol}}^{\text{pol}}(\text{PB}) \rangle^e$	$\langle \Delta G_{\text{sol}}^{\text{pol}}(\text{GB}) \rangle^e$	E^{disp}	$\langle \Delta G_{\text{sol}}^{\text{nonpol}} \rangle^{e,f}$
1	IEM	−4.33	−4.03	−3.95	−78.27	79.45 (6.79)	67.62 (7.06)	−38.88	−5.00 (0.05)
2	HEM	−4.44	−4.44	−4.44	−85.77	78.82 (4.76)	67.35 (5.31)	−37.32	−4.99 (0.05)
3	DEM	−4.05	−4.30	−4.41	−98.06	93.87 (7.66)	80.17 (8.50)	−40.34	−5.08 (0.06)
4	DANA	−5.47	−5.65	−5.86	−154.28	123.44 (9.27)	113.31 (8.93)	−36.81	−4.87 (0.11)
variance ^g					889.36	327.25	351.25	1.92	0.01
5	zanamivir	−6.77	−6.62	−6.38	−247.22	197.14 (7.71)	197.98 (6.05)	−43.03	−5.22 (0.05)
variance ^g					3989.09	1967.09	2429.14	5.06	0.01

^a In kcal/mol. ^b $\Delta G_{\text{obs}} = 2.303 RT \log K_i$ ($T = 310 \text{ K}$). ^c Calculated from eq 1. ^d Calculated from eq 2. ^e Average value and standard deviation (in parentheses). ^f $\Delta G_{\text{sol}}^{\text{nonpol}} = \gamma \Delta \text{ASA}$, where ASA is the water accessible surface area and γ is taken to be $0.0072 \text{ kcal/mol}/\text{\AA}^2$. ^g In $\text{kcal}^2/\text{mol}^2$.

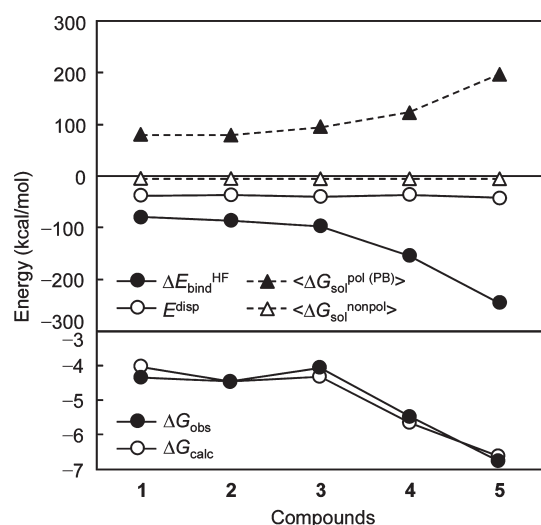


Figure 1. Variations of $\Delta E_{\text{bind}}^{\text{HF}}$, $\langle \Delta G_{\text{sol}}^{\text{pol}}(\text{PB}) \rangle$, E^{disp} , $\langle \Delta G_{\text{sol}}^{\text{nonpol}} \rangle$, ΔG_{obs} , and ΔG_{calc} values (hNEU2). ΔG_{calc} is calculated by eq 1.

The correlation coefficient between $\Delta E_{\text{bind}}^{\text{HF}}$ and $\langle \Delta G_{\text{sol}}^{\text{pol}}(\text{PB}) \rangle$ is -0.996 for compounds 1–5 (-0.988 for compounds 1–4). This means that these two energy terms are dependent on and compensate for each other. The variance of $\Delta E_{\text{bind}}^{\text{HF}}$ for compounds 1–5 is $\sim 200\%$ larger than that of $\langle \Delta G_{\text{sol}}^{\text{pol}}(\text{PB}) \rangle$ ($\sim 270\%$ for compounds 1–4), and the difference between $|\Delta E_{\text{bind}}^{\text{HF}}|$ and $\langle \Delta G_{\text{sol}}^{\text{pol}} \rangle$ is distinctly large for compounds 4 (DANA) and 5 (zanamivir). That is, the stabilization due to $\Delta E_{\text{bind}}^{\text{HF}}$ overwhelms the destabilization due to $\langle \Delta G_{\text{sol}}^{\text{pol}} \rangle$. The sum of $\Delta E_{\text{bind}}^{\text{HF}}$ and $\langle \Delta G_{\text{sol}}^{\text{pol}} \rangle$ is excellently correlated with ΔG_{obs} , as shown in eqs 1 and 2

$$\Delta G_{\text{obs}} = (1 + \beta)(1 - \alpha)(\Delta E_{\text{bind}}^{\text{HF}} + \langle \Delta G_{\text{sol}}^{\text{pol}}(\text{PB}) \rangle) - 4.09$$

$$n = 5, r = 0.979, s = 0.265, F = 68.3, (1 + \beta)(1 - \alpha) = 0.0505 \quad (1)$$

$$\Delta G_{\text{obs}} = (1 + \beta)(1 - \alpha)(\Delta E_{\text{bind}}^{\text{HF}} + \langle \Delta G_{\text{sol}}^{\text{pol}}(\text{GB}) \rangle) - 3.28$$

$$n = 5, r = 0.940, s = 0.439, F = 22.9, (1 + \beta)(1 - \alpha) = 0.0630 \quad (2)$$

Although the statistical quality of eq 1 using PB is slightly better than that of eq 2 using GB, it is probably difficult and mostly pointless to discuss the difference, because each of the two

computing procedures, PB and GB, involves several approximations and parameters. The correlation coefficient between $\langle \Delta G_{\text{sol}}^{\text{pol}}(\text{PB}) \rangle$ and $\langle \Delta G_{\text{sol}}^{\text{pol}}(\text{GB}) \rangle$ is 0.999 , clearly showing that these two $\langle \Delta G_{\text{sol}}^{\text{pol}} \rangle$ values are equivalent in terms of statistical correlation, at least. When compound 5, which shows the largest $|\Delta E_{\text{bind}}^{\text{HF}}|$ and $|\langle \Delta G_{\text{sol}}^{\text{pol}} \rangle|$, is removed ($n = 4$), the statistical qualities of eqs 1 and 2 are poorer but still statistically significant ($r = 0.941$ and 0.914 , respectively). The absolute values of intercept in eqs 1 and 2 are small, 4.09 and 3.28 , respectively. The β values in eqs 1 and 2 are similar, -0.83 and -0.79 , respectively, when α is assumed to be 0.70 .^{49–52} These results indicate that the penalty energy term ΔG_{others} in eq II is nearly proportional to $(\Delta E_{\text{bind}}^{\text{HF}} + \langle \Delta G_{\text{sol}}^{\text{pol}} \rangle)$ and makes a negative contribution to the observed overall free-energy change ΔG_{obs} , as we expected. As noted above, there is an excellent anticorrelation between $\Delta E_{\text{bind}}^{\text{HF}}$ and $\langle \Delta G_{\text{sol}}^{\text{pol}} \rangle$, and the variation of the former overwhelms that of the latter in the current case.

We then attempted to determine the reason why compound 5 has the smallest $\Delta E_{\text{bind}}^{\text{HF}}$ value among compounds 1–5 in terms of structure and interaction. As shown in Table 2, the large variance in $\Delta E_{\text{bind}}^{\text{HF}}$ ($889 \text{ kcal}^2/\text{mol}^2$) among compounds 1–4 arises from differences in fragment A, because these compounds are different only in fragment A. We carefully examined $\Delta E_{\text{bind}}^{\text{HF}}$ arising from interaction of fragment A with pocket A in hNEU2. Figure 2 shows the IFIE^{HF} values of fragment A with amino acid residues in pocket A. Pocket A in hNEU2 consists of Glu111, Tyr179, Tyr181, Leu217, Glu218, and Gln270. The side chain of Glu218 is located in close to fragment A (R_1) but does not form a stable hydrogen-bond with hydroxyl groups in fragment A of compounds 2–4. The weak stabilization of IFIE^{HF} (fragment A, Glu218) commonly found in compounds 1–4 is probably due to the charge (electron) transfer (CT) from negatively charged Glu218 to neutral fragment A in compounds 1–4. In addition to the effect of CT, weak hydrogen-bonding/electrostatic interactions between hydroxyl groups on fragment A in compounds 2–4 and oxygen atoms in the side chain of Glu218 are possibly involved. The IFIE^{HF} (fragment A, pocket A) values for compounds 1 and 2 indicate that fragment A in these compounds does not interact with pocket A effectively. The negative IFIE^{HF} (fragment A/compound 3, Tyr179) value is due to a weak hydrogen-bonding interaction between the side chain of Tyr179 and the OH¹ group in fragment A (distance ($\text{H}^1\text{O} \cdots \text{HO} - \text{Tyr179}$) = 2.04 \AA). The OH¹ group attached to fragment A in compound 4 shows remarkably high attractive interaction energy with Glu111, because the OH¹ group and oxygen atoms in the side chain of Glu111 take on atomic positions optimum for effective

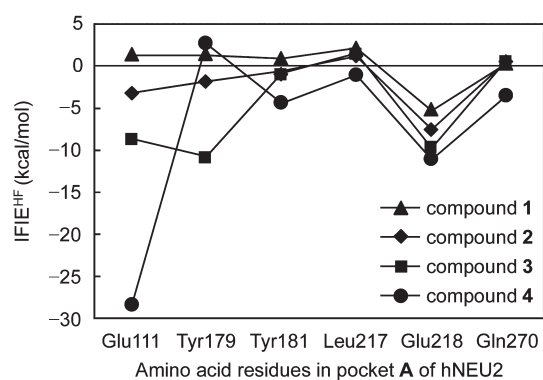


Figure 2. IFIE^{HF} values of fragment A in compounds 1–4 with amino acid residues in pocket A of hNEU2.

hydrogen-bonding and electrostatic interactions [distance ($\text{H}^1\cdots\text{O}-\text{Glu111}$) = 1.54 Å, angle ($\text{O}-\text{H}^1\cdots\text{O}-\text{Glu111}$) = 176 deg, and angle ($\text{H}^1\cdots\text{O}-\text{C}_\delta-\text{Glu111}$) = 116 deg].

The variance analysis of the IFIE^{HF} value between residue X and fragment A in a ligand among compounds 1–4 (denoted as $\text{var}[\text{IFIE}^{\text{HF}}(\text{fragment A}, X)]$) shows that $\text{var}[\text{IFIE}^{\text{HF}}(\text{fragment A}, \text{Glu111})]$, $\text{var}[\text{IFIE}^{\text{HF}}(\text{fragment A}, \text{Tyr179})]$, and $\text{var}[\text{IFIE}^{\text{HF}}(\text{fragment A}, \text{Arg237})]$ are 128.7, 27.1, and 24.8 $\text{kcal}^2/\text{mol}^2$, respectively, and that $\text{var}[\text{IFIE}^{\text{HF}}(\text{fragment A}, X)]$ values other than the above three ones are less than 5.5 $\text{kcal}^2/\text{mol}^2$. This result clearly suggests that these three residues govern the overall variation in the electrostatic interaction energy among compounds 1–4. Glu111 is a key residue which interacts with the OH^1 group (fragment A) in compound 4 through the electrostatic and/or hydrogen-bonding interactions. In addition, Arg237 (pocket B) in close proximity to fragment A significantly contributes to the stabilization of the electrostatic interaction energy with compound 4, but not with compounds 1–3. In fact, $\text{IFIE}^{\text{HF}}(\text{fragment A}, \text{Arg237})$ of compound 4 is 10–13 kcal/mol smaller than those of compounds 1–3. This is because the OH^2 group in compound 4 only takes favorable position for the electrostatic interaction with the positively charged side chain of Arg237.

Fragment A in compound 4 undergoes the largest stabilization through the hydrogen-bonding and electrostatic interactions. Consequently, compound 4 exhibits the most potent inhibitory activity among compounds 1–4.

The above results quantitatively confirm that the hydrogen-bonding interaction energy of fragment A in compounds 1–4 with residues in pocket A mostly determines the observed overall free-energy change and suggest that the position of the hydroxyl group in fragment A is crucial for the optimum hydrogen-bond formation with residues in pocket A. Although the interaction energy of fragment A with amino acid residues in pocket A is not the most important contributor to the stabilization of the total binding energy, it should be noted that the structural factors that stabilize the total binding energy are different from those that govern the variation in the total binding energy among compounds 1–4.

Next, we examined the most potent compound 5 (zanamivir), which has the same skeletal structure (fragment B) as compounds 1–4 but has a positively charged guanidino group instead of a neutral hydroxyl group (fragment C). Notably, compounds 4 and 5 have the same fragment A as well as fragment B structure. Differences in the interaction energy between compounds 4 and 5 are unquestionably attributable to those in fragment C.

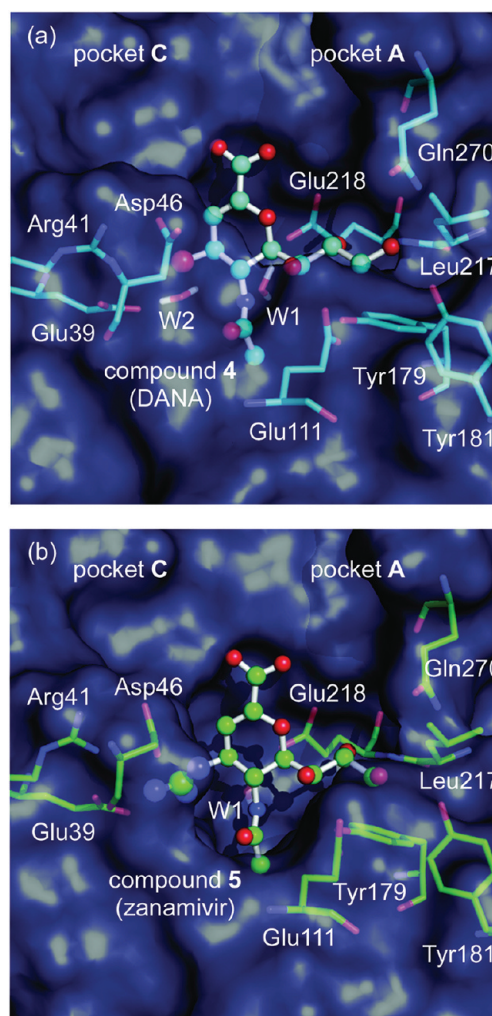


Figure 3. (a) Compound 4 (DANA) and (b) compound 5 (zanamivir) accommodated in the active site of hNEU2.

Figure 3 (a) and (b) shows the structures of compounds 4 and 5 bound at the active site of hNEU2, respectively. The guanidino group (fragment C) in compound 5 is involved in electrostatic interactions with Glu39 and Asp46 in hNEU2, and the corresponding hydroxyl group in compound 4 forms a hydrogen-bond with Arg41.

As can be seen in Figure 4, the $\text{IFIE}^{\text{HF}}(\text{fragment C}/\text{compound 5}, \text{Glu39})$ and $\text{IFIE}^{\text{HF}}(\text{fragment C}/\text{compound 5}, \text{Asp46})$ values represent large negative energies, and the $\text{IFIE}^{\text{HF}}(\text{fragment C}/\text{compound 5}, \text{Arg41})$ value is the positive energy due to the electrostatic repulsive interaction between the positively charged guanidino group and the side chain of Arg41. The relatively small negative $\text{IFIE}^{\text{HF}}(\text{fragment C}/\text{compound 4}, \text{Arg41})$ value represents the hydrogen-bonding interaction, which causes considerably weaker stabilization than electrostatic interactions of the guanidino group in compound 5 with Glu39 and Asp46. In total, $\Delta E_{\text{bind}}^{\text{HF}}$ of compound 5 is 93 kcal/mol more stable than that of compound 4.

3.2. Comparison of Inhibitory Activities of Anti-Influenza Drugs against hNEU2 and N1-NA. Although anti-influenza drugs zanamivir (compound 5) and oseltamivir (compound 6) exhibit excellent inhibitory activity toward various types of influenza virus NAs including N1-NA, their activity toward

hNEU2 is much lower. It is notable that compound **6** has a skeletal structure (fragment **B**) different from that in compounds **1–5**. Table 3 shows the ΔG_{obs} values of compounds **5** and **6** with hNEU2 and N1-NA. The large difference in ΔG_{obs} between compound **5** with hNEU2 and N1-NA as well as that between compound **6** with hNEU2 and N1-NA can be attributed to those between the binding interaction modes of hNEU2 and N1-NA with the two compounds.

The whole protein structures of hNEU2 and N1-NA take on a close topology: six bladed β -propeller folds commonly conserved among neuraminidases are arranged at topologically almost equivalent positions. Although the overall amino acid sequence homology between hNEU2 and N1-NA is considerably low (identity $\sim 16\%$, similarity $\sim 25\%$), several residues in their active sites seem to be conserved: an “arginine triad” (Arg21, 237, and 304 in hNEU2; Arg118, 292, and 371 in N1-NA) and tyrosine (Tyr334 in hNEU2; Tyr406 in N1-NA), which are essential for expression of their catalytic activities. We carefully compared the atomic positions of amino acid residues located in the active sites of the two PDB crystal structures, 1VCU (hNEU2)²¹ and 2HU4 (N1-NA).⁸² Each of the above corresponding pairs of residues takes on nearly the same position in hNEU2 and N1-NA (within 0.76 Å (C_{α} atoms)). Figure 5 (a) and (b) schematically

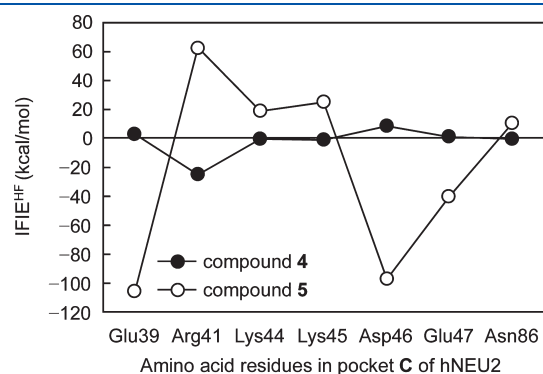


Figure 4. IFIE^{HF} values of fragment C in compounds **4** (DANA) and **5** (zanamivir) with amino acid residues in pocket C of hNEU2.

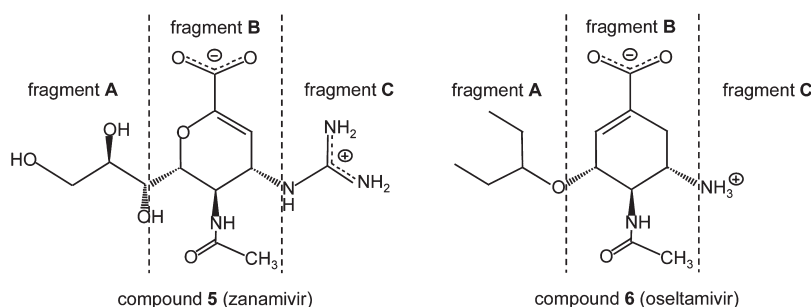
represents the interactions of compound **6** with hNEU2 and N1-NA, respectively.

In pocket **B**, one Tyr and three Arg residues (arginine triad) common in hNEU2 and N1-NA surround a negatively charged carboxylate group in fragment **B** of compound **6**, exhibiting a very close geometry.

A few amino acid residues in pocket **A** are different between hNEU2 and N1-NA. For example, a negatively charged Glu111 in hNEU2 is replaced by nonpolar Ile222 in N1-NA. Although fragment **A** in compound **5** as well as compound **4** form a hydrogen-bond with residues in pocket **A** of hNEU2, fragment **A** in compound **6** is not able to form a hydrogen-bond because it does not have a hydroxyl group. Both compounds **5** and **6** exhibit potent inhibitory potency as to N1-NA, probably because the hydrogen-bonding interaction between fragment **A** and pocket **A** in N1-NA is not dominant, but the dispersion type of interaction (E^{disp} and $\Delta G_{\text{sol}}^{\text{nonpol}}$) governs the interaction energy between fragment **A** and pocket **A** in N1-NA, as demonstrated in our previous study.²⁸

We then examined the differences between the IFIE^{HF} (fragment C (NH_3^+)/compound **6**, pocket C/hNEU2) and IFIE^{HF} (fragment C/compound **6**, pocket C/N1-NA) values. Figure 6 shows the IFIE^{HF} (fragment C/compound **6**, pocket C/hNEU2) and IFIE^{HF} (fragment C/compound **6**, pocket C/N1-NA) values. The $\Sigma\text{IFIE}^{\text{HF}}$ (fragment C, pocket C/hNEU2) and $\Sigma\text{IFIE}^{\text{HF}}$ (fragment C, pocket C/N1-NA) values are mostly due to those of fragment C with ionized residues: negatively charged Glu39 and Asp46 and positively charged Arg41 in hNEU2 and negatively charged Glu119, Asp151, and Glu227 and positively charged Arg156 in N1-NA. Asp46 in hNEU2 and Asp151 in N1-NA stabilize, and Arg41 in hNEU2 and Arg156 in N1-NA destabilize the interaction energy. The above stabilization and destabilization commonly occur in the two complexes. Ile22, Glu39, Met85, and Asn86 in pocket C of hNEU2 are replaced by Glu119, Leu134, Trp178, and Glu227 in N1-NA, respectively. Among the above replacements, that from neutral Ile22 in hNEU2 to negatively charged Glu119 in N1-NA makes the interaction energy of fragment C with N1-NA 105 kcal/mol more stable than that with hNEU2. Similarly, the replacement of Asn86 with Glu227 makes the interaction energy 54 kcal/mol

Table 3. Chemical Structure of Zanamivir and Oseltamivir along with Inhibitory Potency against hNEU2 and N1-NA



compound				ΔG_{obs}^a	
no.	name	R ₁ (fragment A)	R ₂ (fragment C)	hNEU2 ^b	N1-NA ^c
5	zanamivir	CH(OH ¹)CH(OH ²)CH ₂ (OH ³)	NHC(=NH ₂ ⁺)NH ₂	−6.77	−12.80
6	oseltamivir	OCH(CH ₂ CH ₃) ₂	NH ₃ ⁺	−3.26	−13.26

^a In kcal/mol. ^b $\Delta G_{\text{obs}} = 2.303 RT \log K_i$ ($T = 310$ K). K_i value is taken from ref 33. ^c $\Delta G_{\text{obs}} = 2.303 RT \log (\text{IC}_{50})$ ($T = 310$ K). IC_{50} value is taken from ref 81.

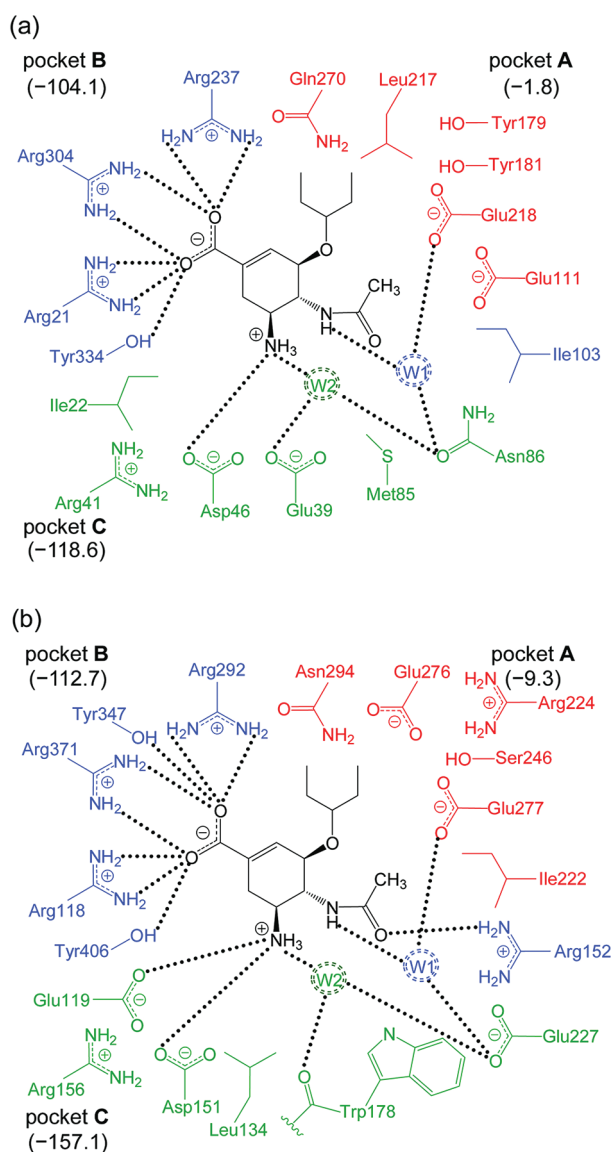


Figure 5. Interaction of compound 6 (oseltamivir) with amino acid residues in the active sites of (a) hNEU2 and (b) N1-NA. $\Sigma\text{IFIE}^{\text{HF}}$ (fragment X, pocket X: X = A (red), B (blue), and C (green)) values are shown in parentheses (kcal/mol). W1 and W2 represent water molecules in the active sites. A dotted line represents an attractive interaction.

more stable. Conversely, the replacement of negatively charged Glu39 with neutral Leu134 stabilizes the complex of hNEU2 with compound 6 by 70 kcal/mol. The energy differences $\Delta\Sigma\text{IFIE}^{\text{HF}}$ ($= \Sigma\text{IFIE}^{\text{HF}}$ (fragment C/compound 6, pocket C/hNEU2) $- \Sigma\text{IFIE}^{\text{HF}}$ (fragment C/compound 6, pocket C/N1-NA)) reaches a stabilization value of 38 kcal/mol.

In summary, compound 6 shows remarkably less inhibitory activity toward hNEU2 than that toward N1-NA, because of differences in pockets A and C between the two proteins.

We finally examined the difference between the inhibitory activities of compounds 5 and 6 with hNEU2. In our previous paper,²⁸ we showed that $\Sigma\text{IFIE}^{\text{HF}}$ (fragment C/compound 6, pocket C/N1-NA) is not far from $\Sigma\text{IFIE}^{\text{HF}}$ (fragment C in the compound where the amino group in compound 6 is replaced by a guanidino one, pocket C/N1-NA) (-157 and -145 kcal/mol, respectively). However, there is a significantly large difference

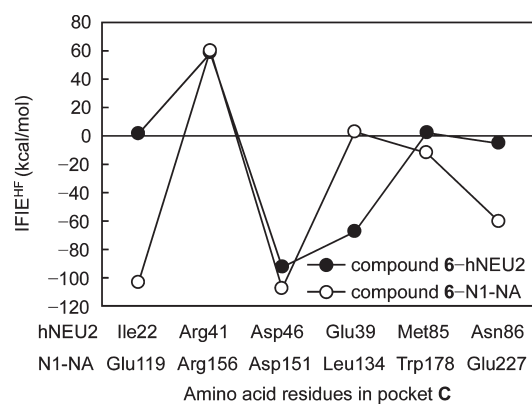


Figure 6. IFIE^{HF} values of fragment C in compound 6 (oseltamivir) with amino acid residues in pocket C of hNEU2 and N1-NA.

between $\Sigma\text{IFIE}^{\text{HF}}$ (fragment C (NH_3^+)/compound 6, pocket C/hNEU2) and $\Sigma\text{IFIE}^{\text{HF}}$ (fragment C ($\text{NHC}(=\text{NH}_2^+)\text{NH}_2$)/compound 5, pocket C/hNEU2). This difference between $\Sigma\text{IFIE}^{\text{HF}}$ (fragment C/compound 6, pocket C/hNEU2) and $\Sigma\text{IFIE}^{\text{HF}}$ (fragment C/compound 5, pocket C/hNEU2) (-119 and -149 , respectively) mostly arises from the interaction energy of fragment C with Glu39 [IFIE^{HF} (fragment C/compound 6, Glu39) and IFIE^{HF} (fragment C/compound 5, Glu39) are -68 (see Figure 6) and -106 (Figure 4) kcal/mol, respectively]. This is because the positively charged guanidino group in compound 5 is located closer to negatively charged Glu39 in hNEU2 than the amino group in compound 6. The nearest interatomic (heavy atoms) distances between Glu39 and fragment C are 2.76 and 4.48 Å for compounds 5 and 6, respectively. The above differences as well as those in the interactions between fragment A and pocket A make the inhibitory activity of compound 6 toward hNEU2 considerably less potent than that of compound 5.

4. SUMMARY AND CONCLUSION

In our previous study,²⁸ we showed that the variation in the inhibitory potency as to N1-NA among eight analogues (including oseltamivir) having alkoxy side chains ($\text{OC}_n\text{H}_{2n+1}$, $n = 0, 3, 4$, and 5) at R_1 (fragment A) is governed by the dispersion (E^{disp}) and/or hydrophobic interaction ($\Delta G_{\text{sol}}^{\text{nonpol}}$) energies. In the present study, we showed that the observed overall free-energy changes of DANA, three analogues of DANA, and an anti-influenza drug zanamivir, all of which have a common skeletal structure (fragment B), are linearly correlated with the calculated one using FMO and MD-PB(GB)/SA calculations (LERE-QSAR). Unlike the case reported in the previous study, the statistical variances of the local energy terms E^{disp} and $\langle \Delta G_{\text{sol}}^{\text{nonpol}} \rangle$ are both 3–6 orders of magnitude smaller than those of the electrostatic energy terms $\Delta E_{\text{bind}}^{\text{HF}}$ and $\langle \Delta G_{\text{sol}}^{\text{pol}} \rangle$. Because of penalty and entropy–enthalpy compensation effects, the coefficient of ($\Delta E_{\text{bind}}^{\text{HF}} + \langle \Delta G_{\text{sol}}^{\text{pol}} \rangle$) in the correlation equations eqs 1 and 2 is considerably smaller than unity (~ 0.05). There is an excellent anticorrelation between the electrostatic energy terms $\Delta E_{\text{bind}}^{\text{HF}}$ and $\langle \Delta G_{\text{sol}}^{\text{pol}} \rangle$ ($r = \sim -0.99$). Comparison of the variances of the two electrostatic energy terms showed that the contribution (stabilization) from the intrinsic binding energy term $\Delta E_{\text{bind}}^{\text{HF}}$ to the overall free-energy change overwhelms that (destabilization) from the polar solvation free-energy term $\langle \Delta G_{\text{sol}}^{\text{pol}} \rangle$. $\Delta E_{\text{bind}}^{\text{HF}}$ can be expressed as the sum of the FMO-IFIE terms for an inhibitor and hNEU2. FMO-IFIE analysis revealed that the

variation in the overall free-energy changes among four sialic acid analogues is determined by hydrogen-bonding interactions between fragment A in a sialic acid analogue and amino acid residues in pocket A in hNEU2. DANA and zanamivir, both of which have the same fragment A structure, show excellent inhibitory activities, because of the effective hydrogen-bond formation of a hydroxyl group in fragment A with Glu111 in hNEU2. The hydroxyl group in fragment C of DANA is replaced by a positively charged guanidino group in zanamivir. This replacement causes great stabilization of the interaction energy through the electrostatic interactions of the guanidino group with negatively charged Glu39 and Asp46, resulting in that zanamivir exhibits more potent activity than DANA.

Second, we determined the reason why an anti-influenza drug, oseltamivir, shows very weak inhibitory activity toward hNEU2, although it exhibits potent activity toward N1-NA. The observed free-energy change for complex formation of hNEU2 with oseltamivir is 10 kcal/mol larger (less stable) than that in the case of N1-NA. There are significant differences in amino acid residues in the active site between the two proteins: notably Ile22, Glu39, and Asn86 in hNEU2 are Glu119, Leu134, and Glu227 in N1-NA, respectively. These three residues surround the hydroxyl and guanidino groups in fragment C of DANA and zanamivir, respectively. IFIE analysis showed that these replacements cause a large difference in the free-energy change between the oseltamivir–hNEU2 and oseltamivir–N1-NA complexes. In addition to the difference in the interaction between fragment C and pocket C, fragment A in oseltamivir, unlike that in zanamivir, is not able to form hydrogen bonds with pocket A. These differences reasonably account for the inefficiency of oseltamivir as to hNEU2.

The present study could provide clues for understanding the neuropsychiatric side effects of oseltamivir, which are similar to the known symptoms of endogenous hNEUs related disorders. Li et al.⁸³ proposed that the hNEU2 variation caused by the Arg41Gln mutation could be associated with the adverse side effects of oseltamivir. They demonstrated that replacement of positively charged Arg41 with neutral Gln41 increases the sensitivity of hNEU2 to oseltamivir and reduces the catalytic activity of hNEU2. This observation is strongly supported by the present results, which suggest that the unfavorable electrostatic repulsive interaction between Arg41 and the positively charged amino group in oseltamivir can be abolished with the mutation from Arg41 to Gln41. In fact, IFIE^{HF} (fragment C, Gln41) is 67 kcal/mol more stable than IFIE^{HF} (fragment C, Arg41) (−9 and 58 kcal/mol, respectively).

The current and previous results²⁸ obtained with the LERE-QSAR analysis successfully reveal the quantitative contribution of each fragment in neuraminidases (hNEU2 and N1-NA) and sialic acid analogues including anti-influenza drugs to the overall interaction free-energy change. Consequently, the results bring a new and consistent understanding of the binding interaction mechanism, which cannot be obtained with any other procedures.

The present work will provide useful information for drug development and for the curing of influenza and other diseases in which neuraminidases are involved.

■ ASSOCIATED CONTENT

S Supporting Information. Atom names, atom types, and partial atomic charges of compounds 1–6. This material is available free of charge via the Internet at <http://pubs.acs.org>.

■ AUTHOR INFORMATION

Corresponding Author

*Phone: +81-88-633-7257. Fax: +81-88-633-9508. E-mail: hchuman@ph.tokushima-u.ac.jp.

■ ACKNOWLEDGMENT

This work was supported by the Ministry of Agriculture, Forestry and Fisheries (Agri-Health Translational Research Project) and Grants-in-Aid for Scientific Research (No. 20590036) from the Ministry of Education, Culture, Sports, Science and Technology.

■ REFERENCES

- (1) Achyuthan, K. E.; Achyuthan, A. M. Comparative enzymology, biochemistry and pathophysiology of human *exo-α*-sialidases (neuraminidases). *Comp. Biochem. Physiol., Part B: Biochem. Mol. Biol.* **2001**, *129*, 29–64.
- (2) De Clercq, E. Antiviral agents active against influenza A viruses. *Nat. Rev. Drug Discovery* **2006**, *5*, 1015–1025.
- (3) von Itzstein, M. The war against influenza: discovery and development of sialidase inhibitors. *Nat. Rev. Drug Discovery* **2007**, *6*, 967–974.
- (4) Liu, Y.; Zhang, J.; Xu, W. Recent progress in rational drug design of neuraminidase inhibitors. *Curr. Med. Chem.* **2007**, *14*, 2872–2891.
- (5) Monti, E.; Preti, A.; Venerando, B.; Borsani, G. Recent development in mammalian sialidase molecular biology. *Neurochem. Res.* **2002**, *27*, 649–663.
- (6) Miyagi, T.; Wada, T.; Yamaguchi, K.; Hata, K. Sialidase and malignancy: a minireview. *Glycoconjugate J.* **2004**, *20*, 189–198.
- (7) Buschiazzi, A.; Alzari, P. M. Structural insights into sialic acid enzymology. *Curr. Opin. Chem. Biol.* **2008**, *12*, 565–572.
- (8) Monti, E.; Bonten, E.; d'Azzo, A.; Bresciani, R.; Venerando, B.; Borsani, G.; Schauer, R.; Tettamanti, G. Sialidases in vertebrates: a family of enzymes tailored for several cell functions. *Adv. Carbohydr. Chem. Biochem.* **2010**, *64*, 403–479.
- (9) Meindl, P.; Tuppy, H. 2-Deoxy-2,3-dehydrosialic acids. II. Competitive inhibition of *Vibrio cholerae* neuraminidase by 2-deoxy-2,3-dehydro-N-acetylneuraminic acids. *Hoppe-Seyler's Z. Physiol. Chem.* **1969**, *350*, 1088–1092.
- (10) Meindl, P.; Bodo, G.; Palese, P.; Schulman, J.; Tuppy, H. Inhibition of neuraminidase activity by derivatives of 2-deoxy-2,3-dehydro-N-acetylneuraminic acid. *Virology* **1974**, *58*, 457–463.
- (11) Holzer, C. T.; von Itzstein, M.; Jin, B.; Pegg, M. S.; Stewart, W. P.; Wu, W.-Y. Inhibition of sialidases from viral, bacterial and mammalian sources by analogues of 2-deoxy-2,3-dihydro-N-acetylneuraminic acid modified at the C-4 position. *Glycoconjugate J.* **1993**, *10*, 40–44.
- (12) Miyagi, T.; Kato, K.; Ueno, S.; Wada, T. Aberrant expression of sialidase in cancer. *Trends Glycosci. Glycotechnol.* **2004**, *16*, 371–381.
- (13) Pshezhetsky, A. V.; Richard, C.; Michaud, L.; Igouda, S.; Wang, S.; Elsliger, M.-A.; Qu, J.; Leclerc, D.; Gravel, R.; Dallaire, L.; Potier, M. Cloning, expression and chromosomal mapping of human lysosomal sialidase and characterization of mutations in sialidosis. *Nat. Genet.* **1997**, *15*, 316–320.
- (14) Monti, E.; Preti, A.; Rossi, E.; Ballabio, A.; Borsani, G. Cloning and characterization of NEU2, a human gene homologous to rodent soluble sialidases. *Genomics* **1999**, *57*, 137–143.
- (15) Wada, T.; Yoshikawa, Y.; Tokuyama, S.; Kuwabara, M.; Akita, H.; Miyagi, T. Cloning, expression, and chromosomal mapping of a human ganglioside sialidase. *Biochem. Biophys. Res. Commun.* **1999**, *261*, 21–27.
- (16) Monti, E.; Bassi, M. T.; Bresciani, R.; Civini, S.; Croci, G. L.; Papini, N.; Riboni, M.; Zanchetti, G.; Ballabio, A.; Preti, A.; Tettamanti, G.; Venerando, B.; Borsani, G. Molecular cloning and characterization of NEU4, the fourth member of the human sialidase gene family. *Genomics* **2004**, *83*, 445–453.

- (17) Miyagi, T. Aberrant expression of sialidase and cancer progression. *Proc. Jpn. Acad., Ser. B* **2008**, *84*, 407–418.
- (18) Pshezhetsky, A. V.; Elsliger, M.-A.; Vinogradova, M. V.; Potier, M. Human lysosomal β -galactosidase-cathepsin A complex: definition of the β -galactosidase-binding interface on cathepsin A. *Biochemistry* **1995**, *34*, 2431–2440.
- (19) Bonten, E. J.; Campos, Y.; Zaitsev, V.; Nourse, A.; Waddell, B.; Lewis, W.; Taylor, G.; d'Azzo, A. Heterodimerization of the sialidase NEU1 with the chaperone protective protein/cathepsin A prevents its premature oligomerization. *J. Biol. Chem.* **2009**, *284*, 28430–28441.
- (20) d'Azzo, A.; Hoogeveen, A.; Reuser, A. J.; Robinson, D.; Galjaard, H. Molecular defect in combined β -galactosidase and neuraminidase deficiency in man. *Proc. Natl. Acad. Sci. U.S.A.* **1982**, *79*, 4535–4539.
- (21) Chavas, L. M. G.; Tringali, C.; Fusi, P.; Venerando, B.; Tettamanti, G.; Kato, R.; Monti, E.; Wakatsuki, S. Crystal structure of the human cytosolic sialidase Neu2. Evidence for the dynamic nature of substrate recognition. *J. Biol. Chem.* **2005**, *7*, 469–475.
- (22) von Itzstein, M.; Wu, W.-Y.; Kok, G. B.; Pegg, M. S.; Dyason, J. C.; Jin, B.; Phan, T. V.; Smythe, M. L.; White, H. F.; Oliver, S. W.; Colman, P. M.; Varghese, J. N.; Ryan, D. M.; Woods, J. M.; Bethell, R. C.; Hotham, V. J.; Cameron, J. M.; Penn, C. R. Rational design of potent sialidase-based inhibitors of influenza virus replication. *Nature* **1993**, *363*, 418–423.
- (23) Kim, C. U.; Lew, W.; Williams, M. A.; Liu, H.; Zhang, L.; Swaminathan, S.; Bischofberger, N.; Chen, M. S.; Mendel, D. B.; Tai, C. Y.; Laver, W. G.; Stevens, R. C. Influenza neuraminidase inhibitors possessing a novel hydrophobic interaction in the enzyme active site: design, synthesis, and structural analysis of carbocyclic sialic acid analogues with potent anti-influenza activity. *J. Am. Chem. Soc.* **1997**, *119*, 681–690.
- (24) Babu, Y. S.; Chand, P.; Bantia, S.; Kotian, P.; Dehghani, A.; El-Kattan, Y.; Lin, T.-H.; Hutchison, T. L.; Elliott, A. J.; Parker, C. D.; Ananth, S. L.; Horn, L. L.; Laver, G. W.; Montgomery, J. A. BCX-1812 (RWJ-270201): discovery of a novel, highly potent, orally active, and selective influenza neuraminidase inhibitor through structure-based drug design. *J. Med. Chem.* **2000**, *43*, 3482–3486.
- (25) Honda, T.; Masuda, T.; Yoshida, S.; Arai, M.; Kobayashi, Y.; Yamashita, M. Synthesis and anti-influenza virus activity of 4-guanidino-7-substituted Neu5Ac2en derivatives. *Bioorg. Med. Chem. Lett.* **2002**, *12*, 1921–1924.
- (26) Hata, K.; Koseki, K.; Yamaguchi, K.; Moriya, S.; Suzuki, Y.; Yingsakmongkon, S.; Hirai, G.; Sodeoka, M.; von Itzstein, M.; Miyagi, T. Limited inhibitory effects of oseltamivir and zanamivir on human sialidases. *Antimicrob. Agents Chemother.* **2008**, *52*, 3484–3491.
- (27) Edwards, E. T.; Truffa, M. M. One-year post pediatric exclusivity postmarketing adverse events review drug: oseltamivir phosphate, 2005. U.S. Food and Drug Administration Centre for Drug Evaluation and Research. http://www.fda.gov/ohrms/dockets/AC/05/briefing/2005-4180b_06_01_Tamiflu%20AE_reviewed.pdf (accessed May 1, 2011).
- (28) Hitaoka, S.; Harada, M.; Yoshida, T.; Chuman, H. Correlation analyses on binding affinity of sialic acid analogues with influenza virus neuraminidase-1 using ab initio MO calculations on their complex structures. *J. Chem. Inf. Model.* **2010**, *50*, 1796–1805.
- (29) Yoshida, T.; Munei, Y.; Hitaoka, S.; Chuman, H. Correlation analyses on binding affinity of substituted benzenesulfonamides with carbonic anhydrase using ab initio MO calculations on their complex structures. *J. Chem. Inf. Model.* **2010**, *50*, 850–860.
- (30) Munei, Y.; Shimamoto, K.; Harada, M.; Yoshida, T.; Chuman, H. Correlation analyses on binding affinity of substituted benzenesulfonamides with carbonic anhydrase using ab initio MO calculations on their complex structures (II). *Bioorg. Med. Chem. Lett.* **2011**, *21*, 141–144.
- (31) Magesh, S.; Moriya, S.; Suzuki, T.; Miyagi, T.; Ishida, H.; Kiso, M. Design, synthesis, and biological evaluation of human sialidase inhibitors. Part 1: selective inhibitors of lysosomal sialidase (NEU1). *Bioorg. Med. Chem. Lett.* **2008**, *18*, 532–537.
- (32) Magesh, S.; Savita, V.; Moriya, S.; Suzuki, T.; Miyagi, T.; Ishida, H.; Kiso, M. Human sialidase inhibitors: design, synthesis, and biological evaluation of 4-acetamido-5-acylamido-2-fluoro benzoic acids. *Bioorg. Med. Chem.* **2009**, *17*, 4595–4603.
- (33) Chavas, L. M. G.; Kato, R.; Suzuki, N.; von Itzstein, M.; Mann, M. C.; Thomson, R. J.; Dyason, J. C.; McKimm-Breschkin, J.; Fusi, P.; Tringali, C.; Venerando, B.; Tettamanti, G.; Monti, E.; Wakatsuki, S. Complexity in influenza virus targeted drug design: interaction with human sialidases. *J. Med. Chem.* **2010**, *53*, 2998–3002.
- (34) Li, Y.; Cao, H.; Yu, H.; Chen, Y.; Lau, K.; Qu, J.; Thon, V.; Sugiarto, G.; Chen, X. Identifying selective inhibitors against the human cytosolic sialidase NEU2 by substrate specificity studies. *Mol. Biosyst.* **2011**, *7*, 1060–1072.
- (35) Case, D. A.; Cheatham, T. E., III; Darden, T.; Gohlke, H.; Luo, R.; Merz, K. M., Jr.; Onufriev, A.; Simmerling, C.; Wang, B.; Woods, R. J. The Amber biomolecular simulation programs. *J. Comput. Chem.* **2005**, *26*, 1668–1688.
- (36) Wang, J.; Cieplak, P.; Kollman, P. A. How well does a restrained electrostatic potential (RESP) model perform in calculating conformational energies of organic and biological molecules? *J. Comput. Chem.* **2000**, *21*, 1049–1074.
- (37) Wang, J.; Wolf, R. M.; Caldwell, J. W.; Kollman, P. A.; Case, D. A. Development and testing of a general Amber force field. *J. Comput. Chem.* **2004**, *25*, 1157–1174.
- (38) Frisch, M. J.; Trucks, G. W.; Schlegel, H. B.; Scuseria, G. E.; Robb, M. A.; Cheeseman, J. R.; Montgomery, J. A., Jr.; Vreven, T.; Kudin, K. N.; Burant, J. C.; Millam, J. M.; Iyengar, S. S.; Tomasi, J.; Barone, V.; Mennucci, B.; Cossi, M.; Scalmani, G.; Rega, N.; Petersson, G. A.; Nakatsuji, H.; Hada, M.; Ehara, M.; Toyota, K.; Fukuda, R.; Hasegawa, J.; Ishida, M.; Nakajima, T.; Honda, Y.; Kitao, O.; Nakai, H.; Klene, M.; Li, X.; Knox, J. E.; Hratchian, H. P.; Cross, J. B.; Bakken, V.; Adamo, C.; Jaramillo, J.; Gomperts, R.; Stratmann, R. E.; Yazyev, O.; Austin, A. J.; Cammi, R.; Pomelli, C.; Ochterski, J. W.; Ayala, P. Y.; Morokuma, K.; Voth, G. A.; Salvador, P.; Dannenberg, J. J.; Zakrzewski, V. G.; Dapprich, S.; Daniels, A. D.; Strain, M. C.; Farkas, O.; Malick, D. K.; Rabuck, A. D.; Raghavachari, K.; Foresman, J. B.; Ortiz, J. V.; Cui, Q.; Baboul, A. G.; Clifford, S.; Cioslowski, J.; Stefanov, B. B.; Liu, G.; Liashenko, A.; Piskorz, P.; Komaromi, I.; Martin, R. L.; Fox, D. J.; Keith, T.; Al-Laham, M. A.; Peng, C. Y.; Nanayakkara, A.; Challacombe, M.; Gill, P. M. W.; Johnson, B.; Chen, W.; Wong, M. W.; Gonzalez, C.; Pople, J. A. Gaussian 03, Revision C.02; Gaussian, Inc.: Wallingford, CT, 2004.
- (39) Bayly, C. I.; Cieplak, P.; Cornell, W. D.; Kollman, P. A. A well-behaved electrostatic potential based method using charge restraints for deriving atomic charges: the RESP model. *J. Phys. Chem.* **1993**, *97*, 10269–10280.
- (40) Singh, U. C.; Kollman, P. A. An approach to computing electrostatic charges for molecules. *J. Comput. Chem.* **1984**, *5*, 129–145.
- (41) Udommaneethanakit, T.; Rungrotmongkol, T.; Bren, U.; Frece, V.; Stanislav, M. Dynamic behavior of avian influenza A virus neuraminidase subtype H5N1 in complex with oseltamivir, zanamivir, peramivir, and their phosphonate analogues. *J. Chem. Inf. Model.* **2009**, *49*, 2323–2332.
- (42) Bren, U.; Martinek, V.; Florián, J. Decomposition of the solvation free energies of deoxyribonucleoside triphosphates using the free energy perturbation method. *J. Phys. Chem. B* **2006**, *110*, 12782–12788.
- (43) Bren, M.; Florián, J.; Mavri, J.; Bren, U. Do all pieces make a whole? Thiele cumulants and the free energy decomposition. *Theor. Chem. Acc.* **2007**, *117*, 535–540.
- (44) Tringali, C.; Papini, N.; Fusi, P.; Croci, G.; Borsani, G.; Preti, A.; Tortora, P.; Tettamanti, G.; Venerando, B.; Monti, E. Properties of recombinant human cytosolic sialidase HsNEU2. The enzyme hydrolyzes monomerically dispersed GM1 ganglioside molecules. *J. Biol. Chem.* **2004**, *279*, 3169–3179.
- (45) Dunitz, J. D. Win some, lose some: enthalpy–entropy compensation in weak intermolecular interactions. *Chem. Biol.* **1995**, *2*, 709–712.

- (46) Gallicchio, E.; Kubo, M. M.; Levy, R. M. Entropy–enthalpy compensation in solvation and ligand binding revisited. *J. Am. Chem. Soc.* **1998**, *120*, 4526–4527.
- (47) Sharp, K. Entropy–enthalpy compensation: fact or artifact? *Protein Sci.* **2001**, *10*, 661–667.
- (48) Freire, E. A thermodynamic approach to the affinity optimization of drug candidates. *Chem. Biol. Drug Des.* **2009**, *74*, 468–472.
- (49) Schwarz, F. P.; Puri, K. D.; Bhat, R. G.; Surolia, A. Thermodynamics of monosaccharide binding to concanavalin A, pea (*Pisum sativum*) lectin, and lentil (*Lens culinaris*) lectin. *J. Biol. Chem.* **1993**, *268*, 7668–7677.
- (50) Gupta, D.; Cho, M.; Cummings, R. D.; Brewer, C. F. Thermodynamics of carbohydrate binding to galectin-1 from Chinese hamster ovary cells and two mutants. A comparison with four galactose-specific plant lectins. *Biochemistry* **1996**, *35*, 15236–15243.
- (51) Swaminathan, C. P.; Surolia, N.; Surolia, A. Role of water in the specific binding of mannose and mannoooligosaccharides to concanavalin A. *J. Am. Chem. Soc.* **1998**, *120*, 5153–5159.
- (52) Gloster, T. M.; Meloncelli, P.; Stick, R. V.; Zechel, D.; Vasella, A.; Davies, G. J. Glycosidase inhibition: an assessment of the binding of 18 putative transition-state mimics. *J. Am. Chem. Soc.* **2007**, *129*, 2345–2354.
- (53) Frederick, K. K.; Marlow, M. S.; Valentine, K. G.; Wand, A. J. Conformational entropy in molecular recognition by proteins. *Nature* **2007**, *448*, 325–329.
- (54) Avbelj, F.; Baldwin, R. L. Origin of the change in solvation enthalpy of the peptide group when neighboring peptide groups are added. *Proc. Natl. Acad. Sci. U.S.A.* **2009**, *106*, 3137–3141.
- (55) Noyes, R. M. Thermodynamics of ion hydration as a measure of effective dielectric properties of water. *J. Am. Chem. Soc.* **1962**, *84*, 513–522.
- (56) Rashin, A. A.; Honig, B. Reevaluation of the Born model of ion hydration. *J. Phys. Chem.* **1985**, *89*, 5588–5593.
- (57) Chuman, H.; Mori, A.; Tanaka, H.; Yamagami, C.; Fujita, T. Analyses of the partition coefficient, log P, using ab initio MO parameter and accessible surface area of solute molecules. *J. Pharm. Sci.* **2004**, *93*, 2681–2697.
- (58) Kukić, P.; Nielsen, J. E. Electrostatics in proteins and protein–ligand complexes. *Future Med. Chem.* **2010**, *2*, 647–666.
- (59) Case, D. A. Normal mode analysis of protein dynamics. *Curr. Opin. Struct. Biol.* **1994**, *4*, 285–290.
- (60) Hayward, S.; Kitao, A.; Go, N. Harmonicity and anharmonicity in protein dynamics: a normal mode analysis and principal component analysis. *Proteins* **1995**, *23*, 177–186.
- (61) Grünberg, R.; Nilges, M.; Leckner, J. Flexibility and conformational entropy in protein–protein binding. *Structure* **2006**, *14*, 683–693.
- (62) Hou, T.; Wang, J.; Li, Y.; Wang, W. Assessing the performance of the MM/PBSA and MM/GBSA methods. I. The accuracy of binding free energy calculations based on molecular dynamics simulations. *J. Chem. Inf. Model.* **2011**, *51*, 69–82.
- (63) Hou, T.; Wang, J.; Li, Y.; Wang, W. Assessing the performance of the molecular mechanics/Poisson Boltzmann surface area and molecular mechanics/generalized Born surface area methods. II. The accuracy of ranking poses generated from docking. *J. Comput. Chem.* **2011**, *32*, 866–877.
- (64) Naïm, M.; Bhat, S.; Rankin, K. N.; Dennis, S.; Chowdhury, S. F.; Siddiqi, I.; Drabik, P.; Sulea, T.; Bayly, C. I.; Jakalian, A.; Purisima, E. O. Solvated interaction energy (SIE) for scoring protein–ligand binding affinities. I. Exploring the parameter space. *J. Chem. Inf. Model.* **2007**, *47*, 122–133.
- (65) Kitaura, K.; Ikeo, E.; Asada, T.; Nakano, T.; Uebayasi, M. Fragment molecular orbital method: an approximate computational method for large molecules. *Chem. Phys. Lett.* **1999**, *313*, 701–706.
- (66) Fedorov, D. G.; Kitaura, K. Extending the power of quantum chemistry to large systems with the fragment molecular orbital method. *J. Phys. Chem. B* **2007**, *111*, 6904–6914.
- (67) Mochizuki, Y.; Yamashita, K.; Fukuzawa, K.; Takematsu, K.; Watanabe, H.; Taguchi, N.; Okiyama, Y.; Tsuboi, M.; Nakano, T.; Tanaka, S. Large-scale FMO-MP3 calculations on the surface proteins of influenza virus, hemagglutinin (HA) and neuraminidase (NA). *Chem. Phys. Lett.* **2010**, *493*, 346–352.
- (68) Mazanetz, M. P.; Ichihara, O.; Law, R. J.; Whittaker, M. Prediction of cyclin-dependent kinase 2 inhibitor potency using the fragment molecular orbital method. *J. Cheminf.* **2011**, *3*, 2.
- (69) Nakano, T.; Mochizuki, Y.; Kato, A.; Fukuzawa, K.; Ishikawa, T.; Amari, S.; Kurisaki, I.; Tanaka, S. Developments of FMO methodology and graphical user interface in ABINIT-MP. In *The Fragment Molecular Orbital Method: Practical Applications to large Molecular Systems*; Fedorov, D. G., Kitaura, K., Eds.; CRC Press: Boca Raton, FL, 2009; pp 37–59.
- (70) Mochizuki, Y.; Nakano, T.; Koikegami, S.; Tanimori, S.; Abe, Y.; Nagashima, U.; Kitaura, K. A parallelized integral-direct second-order Møller–Plesset perturbation theory method with a fragment molecular orbital scheme. *Theor. Chem. Acc.* **2004**, *112*, 442–452.
- (71) Yoshida, T.; Yamagishi, K.; Chuman, H. QSAR study of cyclic urea type HIV-1 PR inhibitors using ab initio MO calculation of their complex structures with HIV-1 PR. *QSAR Comb. Sci.* **2008**, *27*, 694–703.
- (72) Yoshida, T.; Fujita, T.; Chuman, H. Novel quantitative structure–activity studies of HIV-1 protease inhibitors of the cyclic urea type using descriptors derived from molecular dynamics and molecular orbital calculations. *Curr. Comput.-Aided Drug Des.* **2009**, *5*, 38–55.
- (73) Iwata, T.; Fukuzawa, K.; Nakajima, K.; Aida-Hyugaji, S.; Mochizuki, Y.; Watanabe, H.; Tanaka, S. Theoretical analysis of binding specificity of influenza viral hemagglutinin to avian and human receptors based on the fragment molecular orbital method. *Comput. Biol. Chem.* **2008**, *32*, 198–211.
- (74) Ishikawa, T.; Ishikura, T.; Kuwata, K. Theoretical study of the prion protein based on the fragment molecular orbital method. *J. Comput. Chem.* **2009**, *30*, 2594–2601.
- (75) Sawada, T.; Fedorov, D. G.; Kitaura, K. Structural and interaction analysis of helical heparin oligosaccharides with the fragment molecular orbital method. *Int. J. Quantum Chem.* **2009**, *109*, 2033–2045.
- (76) Kollman, P. A.; Massova, I.; Reyes, C.; Kuhn, B.; Huo, S.; Chong, L.; Lee, M.; Lee, T.; Duan, Y.; Wang, W.; Donini, O.; Cieplak, P.; Srinivasan, J.; Case, D. A.; Cheatham, T. E., III. Calculating structures and free energies of complex molecules: combining molecular mechanics and continuum models. *Acc. Chem. Res.* **2000**, *33*, 889–897.
- (77) Massova, I.; Kollman, P. A. Combined molecular mechanical and continuum solvent approach (MM-PBSA/GBSA) to predict ligand binding. *Perspect. Drug Discovery Des.* **2000**, *18*, 113–135.
- (78) Kuhn, B.; Gerber, P.; Schulz-Gasch, T.; Stahl, M. Validation and use of the MM-PBSA approach for drug discovery. *J. Med. Chem.* **2005**, *48*, 4040–4048.
- (79) Li, Y.; Liu, Z.; Wang, R. Test MM-PB/SA on true conformational ensembles of protein–ligand complexes. *J. Chem. Inf. Model.* **2010**, *50*, 1682–1692.
- (80) Sitkoff, D.; Sharp, K. A.; Honig, B. Accurate calculation of hydration free energies using macroscopic solvent models. *J. Phys. Chem.* **1994**, *98*, 1978–1988.
- (81) Gubareva, L. V.; Webster, R. G.; Hayden, F. G. Comparison of the activities of zanamivir, oseltamivir, and RWJ-270201 against clinical isolates of influenza virus and neuraminidase inhibitor-resistant variants. *Antimicrob. Agents Chemother.* **2001**, *45*, 3403–3408.
- (82) Russell, R. J.; Haire, L. F.; Stevens, D. J.; Collins, P. J.; Lin, Y. P.; Blackburn, G. M.; Hay, A. J.; Gamblin, S. J.; Skehel, J. J. The structure of H5N1 avian influenza neuraminidase suggests new opportunities for drug design. *Nature* **2006**, *443*, 45–49.
- (83) Li, C.-Y.; Yu, Q.; Ye, Z.-Q.; Sun, Y.; He, Q.; Li, X.-M.; Zhang, W.; Luo, J.; Gu, X.; Zheng, X.; Wei, L. A nonsynonymous SNP in human cytosolic sialidase in a small Asian population results in reduced enzyme activity: potential link with severe adverse reactions to oseltamivir. *Cell Res.* **2007**, *17*, 357–362.